15

Multi-Dimensional Force Sensor Design for Haptic Human-Computer Interaction

Aiguo Song
Department of Instrument Science and Engineering, Southeast University
P.R.China

1. Introduction

Haptic human-computer interaction (HapHCI) is interaction between a human and a computer with realistic sense of touch. Haptic interaction between human and computer involves solving challenging problems in mechanical design, sensor, actuator, computer graphics, physical-based modelling and rendering algorithm, human capabilities, and other areas. With the increasing applications of HapHCI in virtual reality, teleoperation, rehabilitation, tele-surgery, entertainment, etc, the importance of the sense of touch for human-computer interaction has been widely acknowledged [Gabriel 2006]. For example, in virtual surgery training system, the surgeon controls the surgical tools and characterizes virtual tissues as normal or abnormal through the sense of touch provided by the HapHCI device. Another example is HapHCI based rehabilitation system for post-stroke patient exercise. During active rehabilitation exercise process, it requires accurate damping force control, and during passive rehabilitation exercise process, relatively accurate traction force is necessary.

HapHCI technique usually consists of three fundamental parts: force/tactile measuring, haptic modelling, and haptic display device. Haptic modelling as well as haptic display hardware has been discussed a lot and exploited for ten years particularly in the area of virtual reality. However, so far little attention has been paid to the design of multi-dimensional force sensor for HapHCI, and the existing commercial six degree-of-freedom (DOF) force sensors are designed mainly for industrial robot control, which are too expensive and often over designed for HapHCI in axis and in bandwidth. As an important component in the HapHCI system, multi-dimensional force sensor not only measures the human hand force/torque acted on the interactive hardware device, such as hand-controller, master-manipulator, joystick etc, as a command input the computer, but also provides force/torque information for close-loop control of precise haptic display.

A number of multi-dimensional force sensors have been developed during the past decades, which are intended for use at the end effector of a robot to monitor assembly or machine force. Most of them are six axes force/torque sensors [Watson, Drake, 1975] [Lord Corporation, 1985] [Nakamura et al., 1987] [Kaneko, Nishihara, 1993] [Kim, 2001], which measure three axes forces Fx, Fy, Fz, and three axes torques Mx, My, Mz. And some of them

are three axes force sensors, such as RIXEN EFS-202 [Emplus Corporation, 1991], three-axis gripper force sensor [Kim, 2007], which only measure three axes forces Fx, Fy, Fz.
Although there exist several different types of multi-dimensional force sensors, Lorenze et al pointed out that most of the conventional force sensors are not suitable for use in HapHCI systems, which often over designed for measuring the interaction force between human and machine, and Lorenze et al presented a new type of force sensor for HapHCI, which only measures x and y force components [Lorenze et al, 1999].
This chapter focuses on the multi-dimensional force sensor design for HapHCI. We firstly discuss the role played by the force/torque sensor in the HapHCI systems, and build the dynamics model of the force/torque sensor in the HapHCI. Then we give the general principles of force/torque sensor design for HapHCI. According to the proposed design principles, a novel 4 DOF force/torque sensor for HapHCI is developed, which is designed to measure three axes forces Fx, Fy, Fz, and one axis torque Mz by ignoring the other two axes torques. In this chapter, the mechanical structure of the 4 DOF force/torque sensor is presented, and the strain of the elastic body is analyzed in theory and by FEM analysis software ANSYS, respectively. At last, the calibration results of the 4 DOF force/torque sensor are given. The FEM analysis and calibration results show the new force/torque sensor has low cross sensitivity without decoupling matrix calculation. This 4 DOF force/torque sensor is easier to fabricate with lower cost than the existing commercial force/torque sensors. It is well suitable for use in HapHCI systems.

2. Dynamics model of the force sensor in the HapHCI

A typical haptic human-computer interaction system is show in Figure 1. The human operator holds the human-computer interaction device (e.g. hand controller, master manipulator, Phantom hand, etc.) to control the avatar (e.g. virtual hand, virtual probe, etc.) touch with the virtual objects in virtual environment. The force sensor is usually installed between human hand and the human-computer interaction device, which is used to measure the interactive force between them. The position sensor on the human-computer interaction device acquires three dimensional space position of the human hand as command input to the virtual environment. The computer calculates the interactive force between avatar and virtual objects by using the haptic model and feeds the touch force back to the human hand through the human-computer interaction device.
In general, the HapHCI system in Figure 1 can be represented by the block diagram of Figure 2.

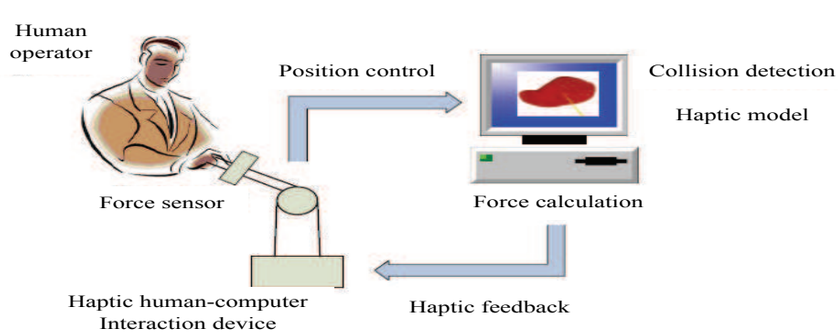

Fig. 1. A typical haptic human-computer interaction system

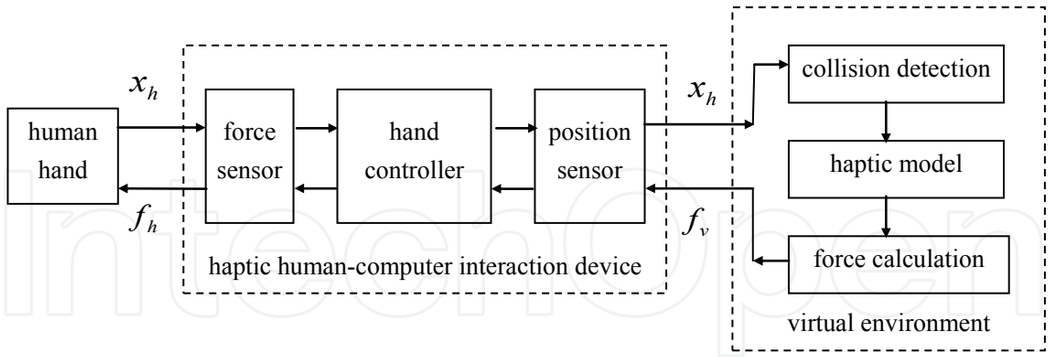

Fig. 2. The block diagram of haptic human-computer interaction system

The dynamics of interaction between human hand and HapHCI system is given as follows.

$$\begin{aligned} f_h - f_v = {} & (M_{fsensor} + M_m + M_{psensor})\ddot{x}_h + (B_{fsensor} + B_m + B_{psensor})\dot{x}_h \\ & + (K_{fsensor} + K_m + K_{psensor})x_h \end{aligned} \tag{1}$$

where x and f denote position and force, respectively; M, B and K denote mass, damp and spring coefficient, respectively; subscript 'fsensor', 'm' and 'psensor' denote the force sensor, hand controller and the position sensor, respectively; fh is interactive force between human hand and HapHCI device, and fv is calculation force by computer based on haptic model. Considering the position sensor is usually relatively very small in size and very light in weight, the equation (1) can be rewritten as

$$f_h - f_v = (M_{fsensor}\ddot{x}_h + B_{fsensor}\dot{x}_h + K_{fsensor}x_h) + (M_m\ddot{x}_h + B_m\dot{x}_h + K_m x_h) \tag{2}$$

For an ideal virtual environment, its dynamics can be expressed as

$$f_v = M_v\ddot{x}_v + B_v\dot{x}_v + K_v x_v \tag{3}$$

$$x_v = x_h \tag{4}$$

According to analogy between mechanical and electrical systems [Anderson, Spong, 1989], equation (3) (4) can be rewritten by using Laplace transformation as follows

$$F_h - F_v = Z_{fsensor}V_h + Z_m V_h \tag{5}$$

$$F_v = Z_v V_v \tag{6}$$

$$V_v = V_h \tag{7}$$

Where, $Z_{fsensor} = M_{fsensor}s + B_{fsensor} + K_{fsensor}/s$ is mechanical impedance of force sensor, $Z_m = M_m s + B_m + K_m / s$ is mechanical impedance of HapHCI device, and $Z_v = M_v s + B_v + K_v / s$ is mechanical impedance of virtual enviroment. $F(s)$ and $V(s)$ are Laplace transforms of $f(t)$, $\dot{x}(t)$, respectively.
Thus, we can represent the HapHCI system as a circuit, shown in Figure 3.

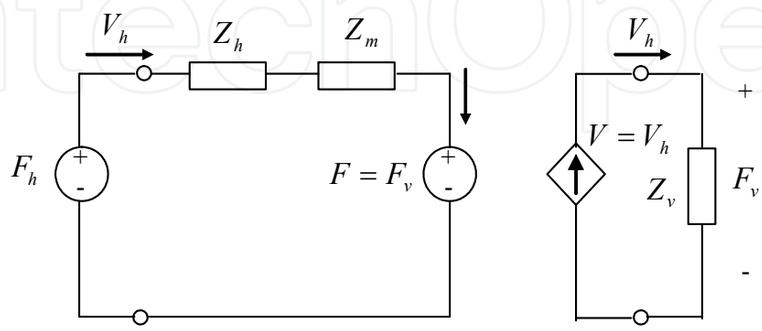

Fig. 3. Circuit representation of HapHCI system

Ideally, human operator can feel as if he is directly touching the virtual environment by maneuvering the HapHCI device, that is to say, the virtual avatar motion $\dot{x}(t)$ equals to the human hand motion $\dot{x}(t)$, and the force of human hand acted on the HapHCI device f_h equals to the virtual interactive force between avatar and virtual object f_v. Lawrence defined the transparency notion for a teleoperation system [Lawrence, 1993]. Here, we extend the transparency notion to evaluate HapHCI system. If a HapHCI system is completely transparent only when it satisfies the condition

$$Z_{feel} \overset{def}{=} \frac{F_h}{V_h} \equiv Z_v \overset{def}{=} \frac{F_v}{V_v} \tag{8}$$

where Z_{feel} is the virtual impedance felt by the human operator.
From equtions (5) (6) (7) (8), we have

$$Z_{feel} = Z_{fsensor} + Z_m + Z_v \tag{9}$$

So it is obvious, reducing the mechanical impedances of force sensor and HapHCI device $Z_{fsensor}$, Z_m can increase the transparency of the HapHCI system, especially when $Z_{fsensor}$, Z_m both equal to zero, the HapHCI system is completely transparent.

Because the damp of force sensors is near zero and stiffness is relatively very high, the mechanical impedance of force sensor is mainly determined by its mass.
Therefore, from the viewpoint of transparency, one of the important requirements of multi-dimensional force sensor design is mass minimization.

3. Principles of force/torque sensor design for HapHCI

Human-computer interaction requires different properties of a force sensor than typical robot applications such as machining and assembly. These differences have substantial impact on how a force sensor can be designed.

3.1 Fewer degrees of freedom required

Owing to the difficulty of mechanical design and motor control for HapHCI device with 6 DOF force feedback, most of the existing HapHCI devices are designed with 3 DOF force feedback, sometimes one torque feedback in addition, although they may be able to move in six directions including 3 DOF translations and 3 DOF rotation.
In spite of six axes force/torque information may be required for some cases in HapHCI systems, the 4 axes force/torque signals, that is three axes forces Fx, Fy, Fz, and one axis torque Mz, are key components of the six axes force/torques, because the torques Mx, My are easy to calculate from the measured forces Fx, Fy and their contact points [Nagarajan et al, 2003]. That is to say the four axes force/torque signals Fx, Fy, Fz, and Mz are sufficient for force sensor design.
Commercial multi-axis force/torque sensors typically measure all six axes forces and torques. In the existing commercial 6 DOF force/torque sensors, there are at least 32 necessary strain gauges stuck to the cross elastic beam, as shown in Figure 4. Owing to difficulty of accurately sticking so many strain gauges to the cross beam, the 6 DOF force/torque sensors usually are very expensive, which restrict their application in HapHCI systems. Another problem of the existing 6 DOF force/torque sensors is coupled interference or noise among six axes, which causes the calibration become much complicate and difficult.

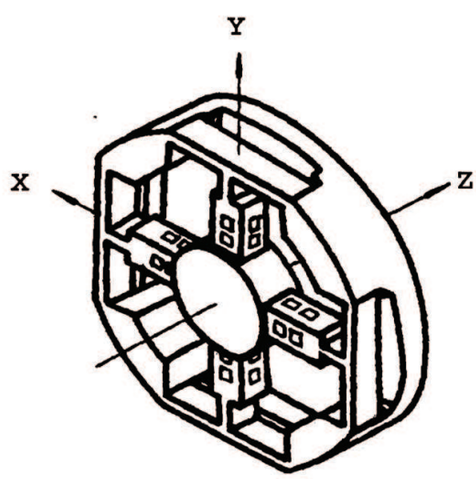

Fig. 4. Mechanical structure of 6 DOF force/torque sensor

3.2 Sensitivity and stiffness requirement

The multi-dimensional force sensor for industrial robot needs very wide bandwidth (more than 1000 Hz bandwidth is often required), which causes the conflict between sensitivity and stiffness during the force sensor design. However, this problem is not faced at all when designing force sensor for HapHCI system. The first reason is the interactive force between human hand and HapHCI device often changes at lower frequency mainly owing to the softness of human hand. The second reason is human is relatively insensitive to small force change and small displacement. So the sensitivity and stiffness of the multi-dimensional force sensor for HapHCI can be lowered a lot (just over 100 Hz bandwidth is needed), which will greatly reduce its expense of fabrication.

3.3 Size and weight requirement

The size and weight of the force/torque sensor for HapHCI is very important. Section 2 has concluded the mass minimization is necessary for force sensor design for HapHCI systems, that means less weight and small size is required. Another reason is that if its diameter is larger or its thickness (length) is longer, it can produce larger inertial force when human hand pulls or pushes the HapHCI devise with a speed, which will reduce both the precision of force measurement and human sense of touch. Furthermore, big size of force sensor will cause it is not easy to install on the existing HapHCI devices (e.g. hand controllers, master manipulators, Phantoms, etc.).

4. A new mechanical structure of the force/torque sensor

We have developed a novel mechanical structure for 6 DOF wrist force/torque sensor before [Huang et al, 1993]. By improving this mechanical structure, we design a new mechanical structure for 4 DOF force/torque sensor for HapHCI [Song et al, 2007], as illustrated in Figure 5.

The elastic body of 4 DOF force/torque sensor consists of center support of the elastic body, cross elastic beam, compliant beams and the base of the elastic body. Where, the cross elastic beam is composed of four symmetric horizontal beams. And four vertical compliant beams connect the four corresponding horizontal beams to the base, respectively.

The whole elastic body is designed to be monolithic and symmetric. Thus, the mechanical structure of the 4 DOF force/torque sensor is light and simple.

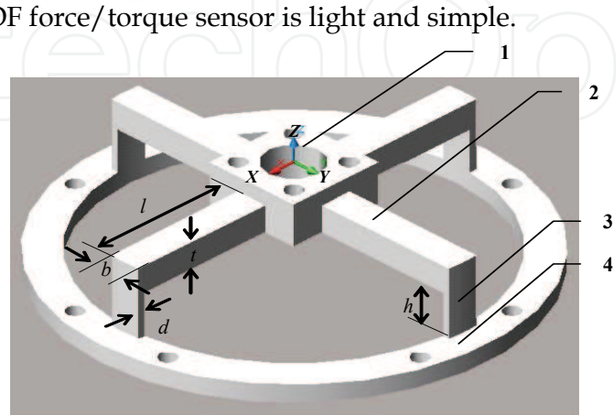

Fig. 5 The mechanical structure for novel force/torque sensor. (1) center support of the elastic body, (2) cross elastic beam, (3) compliance beam, (4) base of the elastic body.

Where, l, b, t are length, width, thickness of the horizontal beam, respectively. And h, d are height, thickness of the vertical compliant beam, respectively. Usually, b=t, $d \le \frac{1}{3}b$.

5. Strain analysis in theory

It can be assumed before analysis that:
(a) The stiffness of the elastic body designed is strong enough for force and moment to be applied. The deformation of the cross elastic beam is within the elastic region for the maximum force and moment applied on it.
(b) The strain gauges are glued correctly, symmetrically and stably.
(c) Every line of the component force passes through the center of the elastic body.
Figure 6 shows the skeleton drawing of the 4 DOF force/torque sensor. When a single force in X direction Fx is applied to the elastic body through its center, the two horizontal beams in X direction OA and OC are float owing to the two vertical beams AA´ and CC´ act as compliant beams, while the other two horizontal beams in Y direction OB and OD become a freely supported beam and produce bending deformation owing to the two vertical beams BB´ and DD´ act as rigid beams.
As is the case for a single force in Y direction Fy, when it is applied to the elastic body through its center, the beams OA and OC become a freely supported beam and produce bending deformation.
When a single force in Z direction Fz is applied to the elastic body through its center, the two horizontal beams OA, OC and two horizontal beams OB, OD become two freely supported beams and produce identical bending deformation.
When a single torque in Z direction Mz is applied to the elastic body through its center, the four horizontal beams OA, OB, OC, OD produce identical bending deformation.

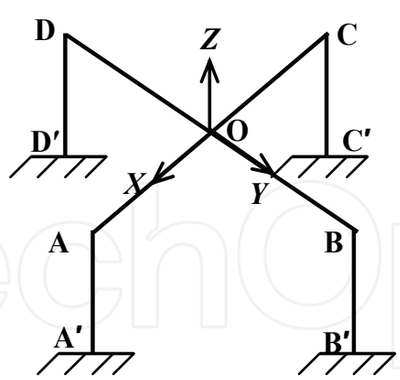

Fig. 6. The skeleton drawing of the sensor

For the novel 4 DOF force/torque sensor, only 16 strain gauges is sufficient for measuring three axes forces and one axis torque, which is twice less than that of 6 DOF force/torque sensor. So it is much easier to stick the strain gauges on the cross elastic beam accurately. Figure 7 depicts skeleton drawing of the distribution of 16 strain gauges on the cross beam.

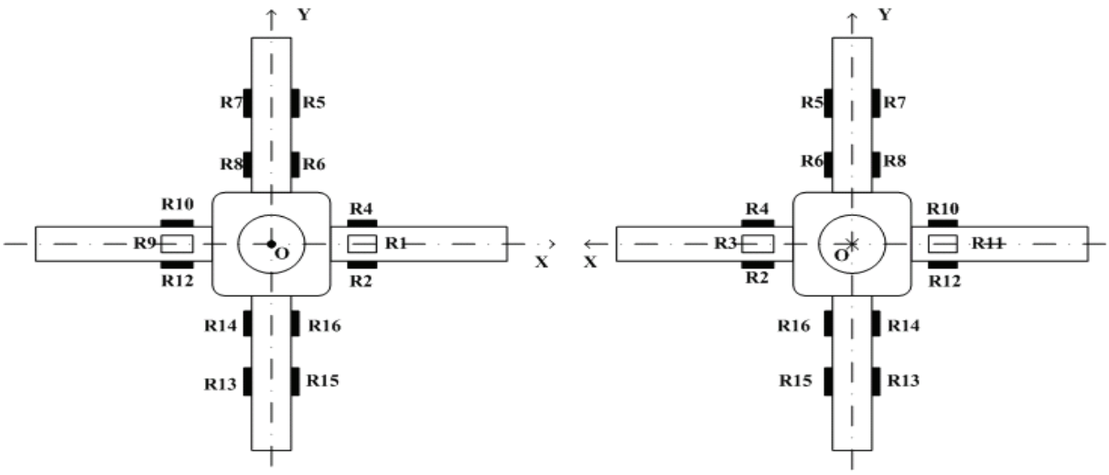

Fig. 7. The distribution of 16 strain gauges on the cross beam

Assuming the strain outputs obtained from the 16 strain gauges R_1, R_2, …,R_{16} are s1, s2, … ,s16, respectively, then we analyze the relationship between the 16 strain outputs and each of the six axes force/torques by using the theory of Mechanism of material.
The 16 strain gauges are divided into four groups and hard wired into four full Wheatstone bridge circuits to measure the four axes force/torques, respectively, as shown in Figure 8.

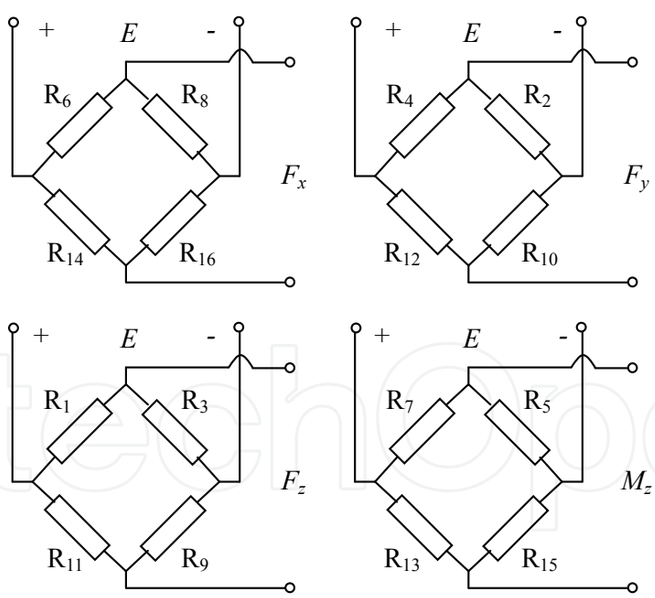

Fig. 8. Four Wheatstone bridge circuits for four axes force/torques measurement

Where, E is voltage of the power supply.
In Reference [Huang, 1993], we have proved an important case of strain gauge output, if a strain gauge is glued at the neutral axis of a beam, when the beam is under bending moment in its flank, the output of the strain gauge is unchanged, as shown in Figure 9.

Here, it is easy to prove another important case of strain gauge output. When a beam is under a torque around its center axis, the output of the strain gauge on its side will increase as a result of the enlargement of gauge length, as shown in Figure 10.

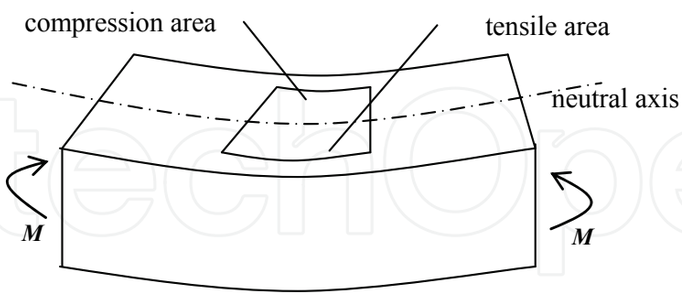

Fig. 9. The beam is under bending moment in its flank

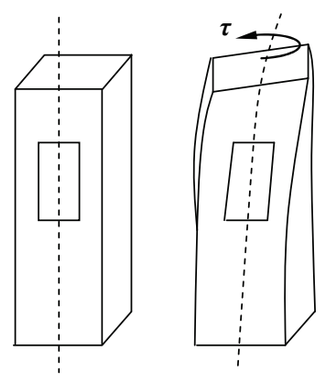

Fig. 10. The beam is under torque moment

From the theory of Mechanics of material, the measured force vector can be easily determined as

$$\mathrm{U_F} = \begin{bmatrix} U_{Fx} \\ U_{Fy} \\ U_{Fz} \\ U_{Mz} \end{bmatrix} = \begin{bmatrix} K_1(s_6 + s_{16} - s_8 - s_{14}) \\ K_2(s_4 + s_{10} - s_2 - s_{12}) \\ K_3(s_1 + s_9 - s_3 - s_{11}) \\ K_4(s_7 + s_{15} - s_5 - s_{13}) \end{bmatrix} \tag{10}$$

here, K_1, K_2, K_3, K_4 are coefficients of the U_{Fx}, U_{Fy}, U_{Fz}, U_{Mz}, respectively, which are determined when the 4 DOF force/torque sensor is designed.

When single one of the six axes force/torques is applied to the sensor, it is not difficult to deduce the relationship between 16 gauge outputs and each of the six axes force/torques from the theory of Mechanics of material. The results are seen in table 1. Here, "+", "-" denote the increment and reduction of gauge output, respectively, and "0" means fixedness.

	Applied force/torques					
	F_x	F_y	F_z	M_z	M_x	M_y
s_1	**0**	**0**	+	**0**	+	-
s_2	**0**	-	**0**	-	+	**0**
s_3	**0**	**0**	-	**0**	+	+
s_4	**0**	+	**0**	+	+	**0**
s_5	+	**0**	**0**	-	**0**	+
s_6	+	**0**	**0**	-	**0**	+
s_7	-	**0**	**0**	+	**0**	+
s_8	-	**0**	**0**	+	**0**	+
s_9	**0**	**0**	+	**0**	+	+
s_{10}	**0**	+	**0**	-	+	**0**
s_{11}	**0**	**0**	-	**0**	+	-
s_{12}	**0**	-	**0**	+	+	**0**
s_{13}	-	**0**	**0**	-	**0**	+
s_{14}	-	**0**	**0**	-	**0**	+
s_{15}	+	**0**	**0**	+	**0**	+
s_{16}	+	**0**	**0**	+	**0**	+

Table 1. The gauge output changes under each applied force/torque

Substituting the data in table 1 into equation (1) yields the outputs of the sensor under six axis force/torques, shown in Table 2. Table 2 indicates that in theory there is no any coupled interference among six axis force/torques in the sensor, which implies the novel elastic body is mechanically decoupled.

	Applied force/torques					
	F_x	F_y	F_z	M_z	M_x	M_y
U_{Fx}	$4K_1s_6$	0	0	0	0	0
U_{Fy}	0	$4K_2s_4$	0	0	0	0
U_{Fz}	0	0	$4K_3s_1$	0	0	0
U_{Mz}	0	0	0	$4K_4s_7$	0	0

Table 2. Outputs of the sensor

6. Coupled interference analysis by using Finite Element Method

Finite Element Analysis Method (FEM) as the name implies can be used for exact analysis of the elasticity problems. We use the commercial FEM software called ANSYS, produced by ANSYS Corporation, USA, to analyze the coupled interference of the new 4 DOF force/torque sensor.

6.1 Finite element model of the elastic body

The discretization of the domain into sub-regions is the first of a series of steps that must be performed for FEM. The subdivision is usually called mesh generation, and a finite number

of sub-domains are called elements. The discretization of the body involves the decision as to the element number, size and shape of sub-regions used to model the real body.
We discrete the elastic body of the 4 DOF force/torque sensor into sub-regions by using ANASYS software. Here, the element type is set as SOLID95 high-precision element available in the ANSYS, which is much suitable for analysis of bending and twisting of the elastic beam. And the Smart-Size function of the ANSYS is used for mesh generation control. Figure 11 shows a FEM model of the elastic body of the sensor with 49720 element nodes and 28231 elements after mesh generation.

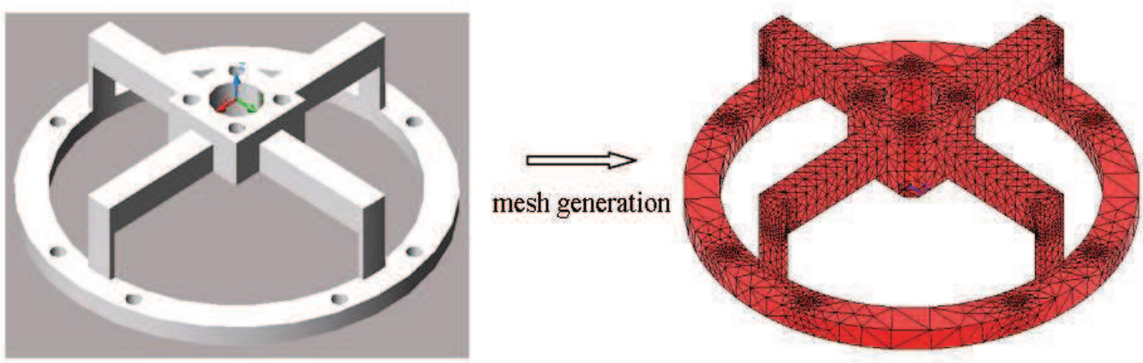

(a) (b)

Fig. 11. Discretization of the elastic body into sub-regions. (a) elastic body of the 4 DOF force/torque sensor, (b) finite element model of the elastic body

The material of the elastic body is aluminium with the parameters as follows:
Young's modulus is 72×10^9 Pa, Poisson ratio is 0.33, and density is 2.78×10^3 kg/m^3.
The size of the elastic body is shown in Table 3.

	Cross elastic beam	Compliant beam	Center support
length (mm)	l=21	h=7	14
width (mm)	b=4.5	b=4.5	14
thickness (mm)	t=4.5	d=1.3	9.5

Table 3. Size of the elastic body

6.2 Strain analysis under six axes force/torques

(1) bound condition set
The elastic body is fixed on the shell of the force/torque sensor through eight bolts on the base, so the connection between them can be regarded as rigid connection. Therefore the total degree of freedom of the base of the elastic body can be set as zero.
(2) applied force/torques
Each single one of the six axis force/torques is applied to the elastic body through its center, respectively. When a single force or torque is applied to the elastic body, the overall

deformation of the elastic body is easy to calculate by using the ANSYS software. What we care about is the strain outputs at the 16 points on the cross beam, to which the 16 strain gauges are stuck, shown in Figure 7. In section 5, we have assumed that s_1, s_2, ……, s_{16} are strain outputs of 16 strain gauges, respectively. The strain of the tensile surface of the beam is defined as positive strain, and the strain of the compressed surface is defined as negative strain.

The measurement range of the analyzed 4 DOF force/torque sensor is designed as F_x =±20N, F_y =±20N, F_z =±20N, M_z =±20×4.5 $N.mm$, respectively.

Because the structure of elastic body is symmetric, the strain circumstance under the single force F_x, is similar to that of F_y, and the strain circumstance under the single torque M_x is similar to that of M_y. For simplification of analysis, we only analyze the strain outputs under each one of the force/torques F_y, F_z, M_z, M_x, respectively.

For the convenience of FEM analysis, the applied force/torques to elastic body are chosen as the maximum 20N or 20×4.5 N.mm.

(3) analysis results of FEM

We apply single force F_y=20N, F_z=20N, and single torque M_z=20×4.5$N.mm$, M_x=20×4.5$N.mm$ on the sensor, respectively. The deformations of the elastic body under each single force/torque calculated by the FEM software are shown in Figure 12, and the strain outputs are seen in the Table 4.

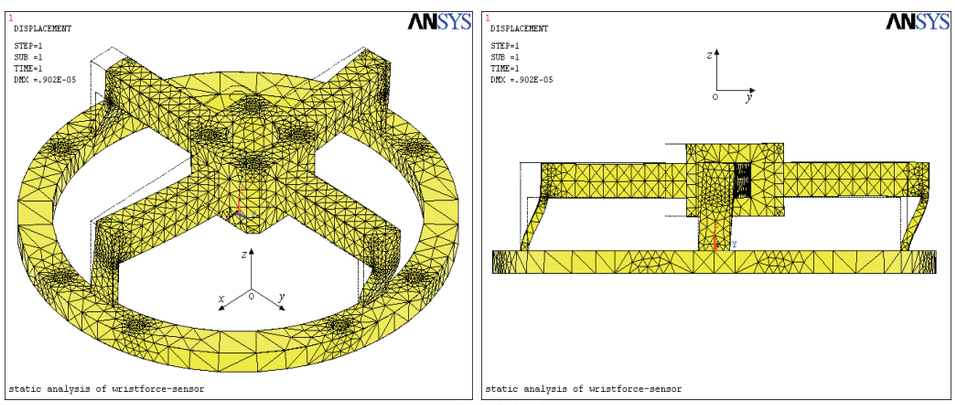

(a) F_y=20N

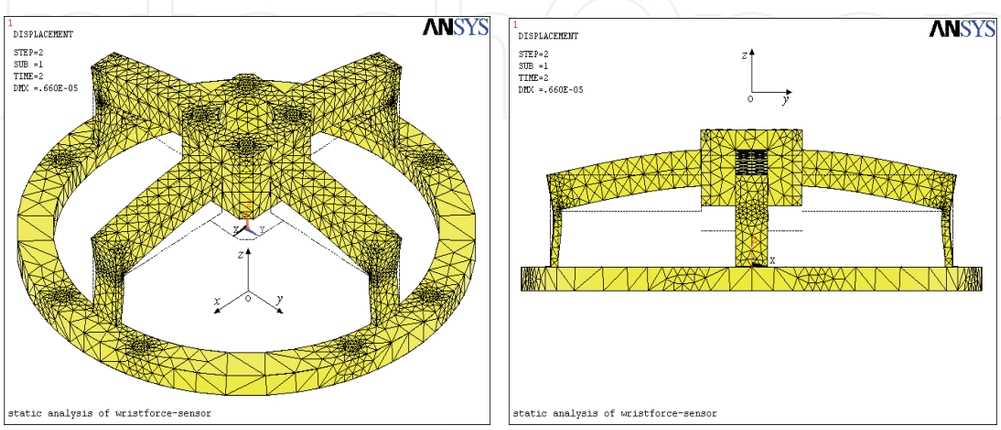

(b) F_z=20N

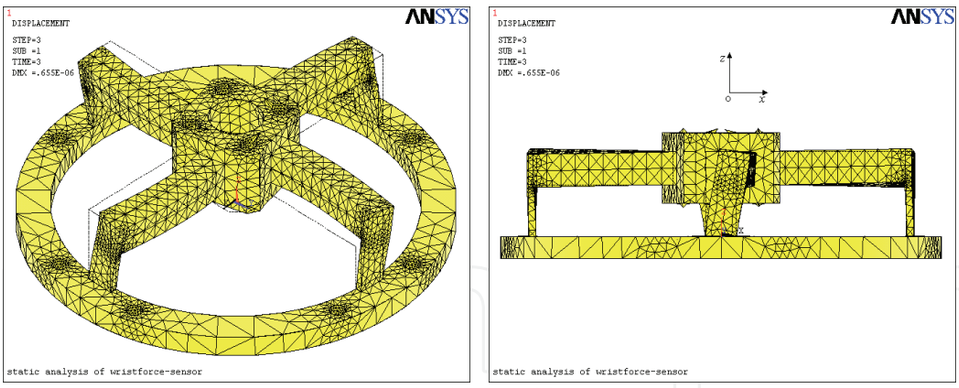

(c) M_z=20×4.5 N.mm

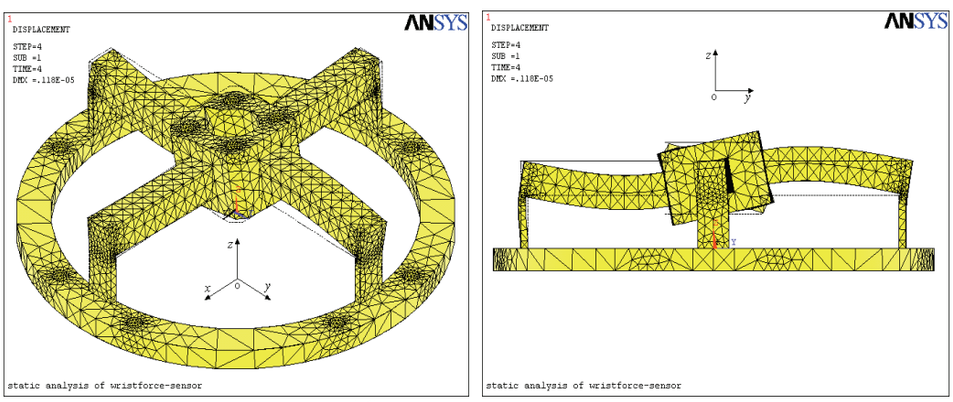

(d) M_x =20×4.5 N.mm

Fig. 12. Deformation of the elastic body under each single force/torque

	F_y=20N	F_z=20N	M_z=90 N.mm	M_x=90N.mm
s_1	0.29	76.16	0.02	0.67
s_2	-74.06	1.20	-13.84	3.08
s_3	0.39	-71.94	0.01	0.60
s_4	74.03	1.30	13.83	3.14
s_5	-4.1	1.07	-10.34	0.22
s_6	-4.1	1.16	-13.84	0.24
s_7	-4.02	0.92	10.42	0.22
s_8	-4.02	0.97	13.91	0.25
s_9	1.07	74.20	-0.19	0.75
s_{10}	73.84	1.12	-13.82	3.11
s_{11}	0.48	-74.66	-0.08	0.72
s_{12}	-73.82	0.81	13.77	3.00
s_{13}	4.04	1.21	-10.54	-0.17
s_{14}	4.04	1.27	-13.60	-0.20
s_{15}	4.05	1.08	10.65	-0.18
s_{16}	4.05	1.16	13.55	-0.21

Table 4. The strain outputs under each single force/torque

6.3 Coupled error analysis of the 4 DOF force/torque Sensor

Substituting the strain outputs under each single force/torque in Table 4 into the equation (10) yields the output matrix as

$$\begin{bmatrix} U_{Fx} \\ U_{Fy} \\ U_{Fz} \\ U_{Mz} \end{bmatrix} = \begin{bmatrix} 295.75K_1 & -0.07K_1 & 0.08K_1 & -0.02K_1 & 0.17K_1 & -0.6K_1 \\ -0.07K_2 & 297.5K_2 & 0.31K_2 & 0.17K_2 & -0.02K_2 & 0.08K_2 \\ 0.49K_3 & 0.49K_3 & 29696K_3 & 0.01K_3 & 0.01K_3 & -0.1K_3 \\ 0.09K_4 & 0.09K_4 & -0.28K_4 & 41.95K_4 & -0.01K_4 & -0.01K_4 \end{bmatrix} \begin{bmatrix} F_x \\ F_y \\ F_z \\ M_x \\ M_y \\ M_z \end{bmatrix} \tag{11}$$

Therefore, the coupled interference under each single force/torque can be easy to calculated. Under a single force F_y=20N, the coupled interference caused by F_y are calculated as follows

$$\begin{aligned} Er(F_x \mid F_y) &= K_1(s_6 + s_{16} - s_8 - s_{14}) = -0.07K_1 \\ Er(F_z \mid F_y) &= K_3(s_1 + s_9 - s_3 - s_{11}) = 0.49K_3 \\ Er(M_z \mid F_y) &= K_4(s_7 + s_{15} - s_5 - s_{13}) = 0.09K_4 \end{aligned}$$

Under a single force F_z=20N, the coupled interference caused by F_z are calculated as follows

$$\begin{aligned} Er(F_x \mid F_z) &= K_1(s_6 + s_{16} - s_8 - s_{14}) = 0.08K_1 \\ Er(F_y \mid F_z) &= K_2(s_4 + s_{10} - s_2 - s_{12}) = 0.31K_2 \\ Er(M_z \mid F_z) &= K_4(s_7 + s_{15} - s_5 - s_{13}) = -0.28K_4 \end{aligned}$$

Under a single torque M_z=20×4.5 $N.mm$, the coupled interference caused by M_z are calculated as follows

$$\begin{aligned} Er(F_x \mid M_z) &= K_1(s_6 + s_{16} - s_8 - s_{14}) = -0.6K_1 \\ Er(F_y \mid M_z) &= K_2(s_4 + s_{10} - s_2 - s_{12}) = 0.08K_2 \\ Er(F_z \mid M_z) &= K_3(s_1 + s_9 - s_3 - s_{11}) = -0.1K_3 \end{aligned}$$

Under a single torque M_x=20×4.5 $N.mm$, the coupled interference caused by M_x can be calculated as follows

$$\begin{aligned} Er(F_x \mid M_x) &= K_1(s_6 + s_{16} - s_8 - s_{14}) = -0.02K_1 \\ Er(F_y \mid M_x) &= K_2(s_4 + s_{10} - s_2 - s_{12}) = 0.17K_2 \\ Er(F_z \mid M_x) &= K_3(s_1 + s_9 - s_3 - s_{11}) = 0.1K_3 \\ Er(M_z \mid M_x) &= K_4(s_7 + s_{15} - s_5 - s_{13}) = -0.01K_4 \end{aligned}$$

For each axis force/torque measurement, the maximum error caused by coupled interference from other 5 axes is usually expressed as a percentage of full scale.

$$Er(F_x) = \frac{|Er(F_x \mid F_y)| + |Er(F_x \mid F_z)| + |Er(F_x \mid M_x)| + |Er(F_x \mid M_y)| + |Er(F_x \mid M_z)|}{full \quad scale \quad of \quad F_x}$$

$$= \frac{K_1(0.07 + 0.08 + 0.02 + 0.17 + 0.60)}{K_1(74.06 + 74.03 + 73.84 + 73.82)} = 0.32\% F.S.$$

$$Er(F_y) = \frac{|Er(F_y \mid F_x)| + |Er(F_y \mid F_z)| + |Er(F_y \mid M_x)| + |Er(F_y \mid M_y)| + |Er(F_y \mid M_z)|}{full \quad scale \quad of \quad F_y}$$

$$= \frac{K_2(0.07 + 0.31 + 0.17 + 0.02 + 0.08)}{K_2(74.06 + 74.03 + 73.84 + 73.82)} = 0.22\% F.S.$$

$$Er(F_z) = \frac{|Er(F_z \mid F_x)| + |Er(F_z \mid F_y)| + |Er(F_z \mid M_x)| + |Er(F_z \mid M_y)| + |Er(F_z \mid M_z)|}{full \quad scale \quad of \quad F_z}$$

$$= \frac{K_3(0.49 + 0.49 + 0.01 + 0.01 + 0.10)}{K_3(76.16 + 71.94 + 74.20 + 74.66)} = 0.37\% F.S.$$

$$Er(M_z) = \frac{|Er(M_z \mid F_x)| + |Er(M_z \mid F_y)| + |Er(M_z \mid F_z)| + |Er(M_z \mid M_x)| + |Er(M_z \mid M_y)|}{full \quad scale \quad of \quad M_z}$$

$$= \frac{K_4(0.09 + 0.09 + 0.28 + 0.01 + 0.01)}{K_4(10.42 + 10.65 + 10.34 + 10.54)} = 1.14\% F.S.$$

Thus, the maximum coupled error of the 4 DOF force/torque sensor is 1.14%F.S. The analysis results of the FEM, which show the proposed elastic body has merit of low coupled interference, are consistent with the theory analysis results in section 3.

7. Calibration test results

Figure 13 shows the prototypes of 4 DOF force/torque sensor fabricated in our Lab, which is designed with force measurement range ±20N, and torque measurement range ±20×4.5 *N.mm*.

(a)

(b)

Fig. 13. Photographs of the 4 DOF force/torque sensors. (a) inner mechanical structure and circuits of the 4 DOF force/torque sensor, (b) two prototypes of 4 DOF force/torque sensor

The relationship between the measurand and the output signal is usually obtained by calibration tests.

The calibration procedure of the force/torque sensor is performed as follows. We apply single one of the 4 DOC force/torques on the sensor with a series of values changed from the minimum to the maximum, respectively. And in the meantime, we set other five axes force/torques to be fixed values. After a round of measurement of 4 DOC force/torques, we set the other five axes force/torques to be new fixed values, and do the same measurement again.

Figure 14 shows the calibration test results. Here, when one axis force/torque is calibrated, the other five axes force/torques are set at zero, half of their full scale values, full scale values, respectively.

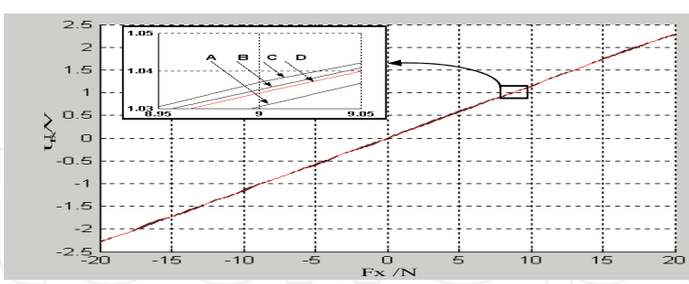

(a)

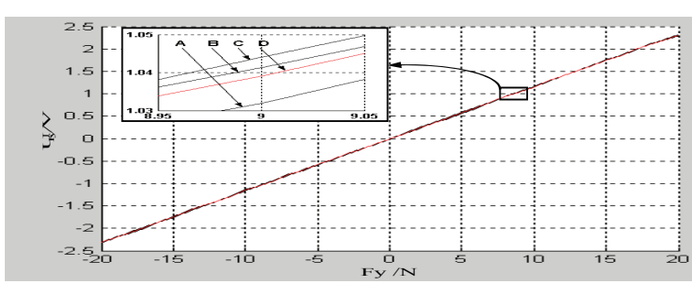

(b)

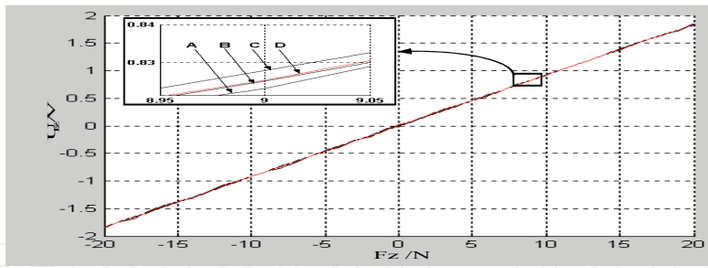

(c)

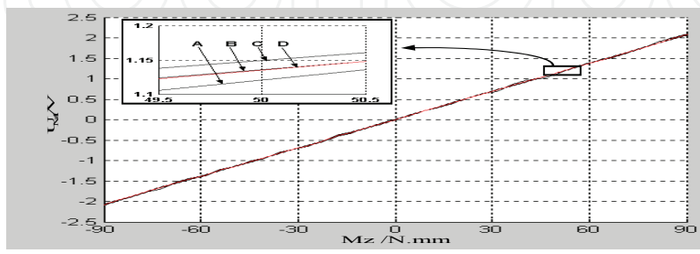

(d)

Fig. 14. Calibration test results. (a) the other five axes force/torques are set at zero, (b) the other five axes force/torques are set at half of full scale values, (c) the other five axes force/torques are set at full scale values, (d) fit curve of average measured values

The calibration results indicate the error of F_x measurement is 0.5%F.S., the error of F_y measurement is 0.5%F.S., the error of F_z measurement is 0.7%F.S., and the error of M_z measurement is 1.3%F.S. Thus the measurement error of the 4 DOF less than 1.5%F.S. (The measurement error of existing commercial 6 DOF force/torque sensors is usually large than 10% F.S. if without decoupling matrix calculation). Although the above error consists not only the coupled interference, but also some other interferences such as error of strain gauge sticking, circuit noise, etc., it is clear that the calibration test results are well correspond with the analysis results of FEM.

The result of impulse response experiment on the 4 DOF force sensor indicates its bandwidth is 210 Hz [Qin, 2004]. Although it is lower than that of the commercial 6 DOF force sensor, it completely meets the bandwidth requirement of HapHCI (>100Hz).

8. Conclusion

A new type multi-dimensional force sensor design for HapHCI is described in this chapter. We build the dynamics model of the force sensor in the HapHCI and give the general principles of force/torque sensor design for HapHCI. According to the proposed design principles, a novel 4 DOF force/torque sensor for HapHCI is developed, which is designed to measure three axis forces Fx, Fy, Fz, and one axis torque Mz by ignoring the other two axis torques. In this chapter, the mechanical structure of the 4 DOF force/torque sensor is presented, and the strain of the elastic body is analyzed in theory and by FEM analysis software ANSYS, respectively. The FEM analysis and calibration results show the new force/torque sensor has low cross sensitivity without decoupling matrix calculation, which means the new force/torque sensor is mechanically decoupled. This new 4 DOF

force/torque sensor can be made much smaller owing to the number of the glued strain gauges is greatly reduced and is easier to construct with much lower cost than the existing commercial force/torque sensors. It is well suitable for measuring multi-dimensional interactive force between human hand and interaction device in HapHCI systems.

9. Acknowledgement

This work was supported by National Basic Research and Development Program of China (No.2002CB312102), National Nature Science Foundation of China (No.60775057), and 863 High-Tec Plan of China (No. 2006AA04Z246).

10. References

Anderson, R.J., Spong M.W. (1989). Bilateral control of teleoperators with time delay. *IEEE Transactions on Automatic Control*, 34, 5, 494-901.

Emplus Corporation (1991). Emplus Technical Note: RIXEN EFS-202

Gabriel, R. (2006). The importance of the sense of touch in virtual and real environments. *IEEE MultiMedia*, 7, 24-30.

Huang, W.Y., Jiang, H.M., Zhou, H.Q. (1993). Mechanical analysis of a novel six-degree-of freedom wrist force sensor. *Sensor and Actuators A: Physical*, 35, 203-208

Kaneko, M. (1993). Twin-head type six-axis force sensors. In *Proceedings of IEEE/RSJ International Conference on Intelligent Robots and Systems*, Yokohama, Japan, pp.26-30.

Kim, G.S. (2001). The design of a six-component force/moment sensor and evaluation of its uncertainty. *Measurement Science and Technology*, 12, 1445-1455.

Kim, G.S. (2007). Development of a three-axis gripper force sensor and the intelligent gripper using it. Sensors and Actuators A: Physical, 137, 2, 213-222.

Lawrence, D.A. (1993). Stability and transparency in bilateral teleoperation. *IEEE Transactions on Robotics and Automation*, 9, 5, 624-637.

Lord Corporation (1985). Force/torque wrist sensing systems. *Technical Note F/T series*. 6-12.

Lorenze, W.A., Peshkin, M.A., Colgate, J.E. (1999). New sensors for new applications: force sensors for human/robot interaction. In *Proceedings of IEEE International Conference on Robotics and Automation*, Detroit, MI, USA, pp.2855-2860.

Nagarajan, R., Sazali, Y., Muralindran, (2003). A design methodology of wrist force sensor for a robot with insufficient degree of freedom. In *Proceedings of IEEE Sensors*, Toronto, Ont., Canada, 22-24 Oct, pp.578-583

Nakamura, Y., Yoshikawa, T., Futamata, I. (1987). Design and signal processing of six axis force sensor. In *Proceedings of 4th International Symposium on Robotics Research*, Santa Barbara, the MIT press, Cambridge, MA

Qin, G., (2004). Research on a novel multi-dimensional wrist force/torque sensor, *Master thesis*, Southeast University, China, (in Chinese)

Song, A.G., Wu, J., Qin G., Huang, W.Y. (2007). A novel self-decoupled four degree-of-freedom wrist force/torque sensor. *Measurement*, 40, 883-891.

Watson, P.C., Drake S.H. (1975). Pedestal and wrist force sensors for automatic assembly. In *Proceedings of 5th International Symposium on Industrial Robot*, pp.501-512.

Human Computer Interaction

Edited by Ioannis Pavlidis

ISBN 978-953-7619-19-0

Hard cover, 522 pages

Publisher InTech

Published online 01, October, 2008

Published in print edition October, 2008

This book includes 23 chapters introducing basic research, advanced developments and applications. The book covers topics such us modeling and practical realization of robotic control for different applications, researching of the problems of stability and robustness, automation in algorithm and program developments with application in speech signal processing and linguistic research, system's applied control, computations, and control theory application in mechanics and electronics.

How to reference

In order to correctly reference this scholarly work, feel free to copy and paste the following:

Aiguo Song (2008). Multi-Dimensional Force Sensor Design for Haptic Human-Computer Interaction, Human Computer Interaction, Ioannis Pavlidis (Ed.), ISBN: 978-953-7619-19-0, InTech, Available from: http://www.intechopen.com/books/human_computer_interaction/multi-dimensional_force_sensor_design_for_haptic_human-computer_interaction

INTECH
open science | open minds

InTech Europe
University Campus STeP Ri
Slavka Krautzeka 83/A
51000 Rijeka, Croatia
Phone: +385 (51) 770 447
Fax: +385 (51) 686 166
www.intechopen.com

InTech China
Unit 405, Office Block, Hotel Equatorial Shanghai
No.65, Yan An Road (West), Shanghai, 200040, China
中国上海市延安西路65号上海国际贵都大饭店办公楼405单元
Phone: +86-21-62489820
Fax: +86-21-62489821